Soft Matter

PAPER

Cite this: *Soft Matter*, 2014, **10**, 8711

Dielectric relaxations of poly(*N*-isopropylacrylamide) microgels near the volume phase transition temperature: impact of cross-linking density distribution on the volume phase transition†

Wenjuan Su,[a] Kongshuang Zhao,*[a] Jingjing Wei[b] and To Ngai[b]

Dielectric relaxation behaviors of three types of thermally sensitive poly(*N*-isopropylacrylamide) (PNIPAM) microgels with different cross-linking density distributions were investigated in a frequency range from 40 Hz to 110 MHz at temperatures from 15 °C to 55 °C. After eliminating the electrode polarization at low frequency, two remarkable relaxations were observed, one in the kHz frequency range and the other in the MHz range. The low-frequency relaxation is attributed to the counterion polarization in the whole measuring temperature range, while the relaxation at high-frequency is probably dominated by different polarization mechanisms depending on below or above the volume phase transition temperature (VPTT): it is considered as micro-Brownian motion of side groups of PNIPAM when T < VPTT and interfacial polarization when T > VPTT. The temperature dependence of the dielectric parameters for both the relaxations presents an abrupt change around 32.5 °C, indicating the occurrence of phase transition. Based on the analysis and discussion about the micro-Brownian motion of the side groups, a possible microstructure for the microgels before and after the collapse of PNIPAM was suggested. A dielectric model to describe the collapsing microgel suspension was proposed, from which the electrical and structural parameters of the suspension were calculated. The information on the internal structure and hydration dynamic behavior of microgels was obtained by using the thermodynamic parameters which were calculated based on the Eyring equation. Our results reveal that the spatial distribution of the cross-linking density distribution has almost no effect on the volume phase transition temperature, but markedly affects the swelling capacity of PNIPAM microgels at low temperatures.

Received 10th July 2014
Accepted 2nd September 2014

DOI: 10.1039/c4sm01516a

www.rsc.org/softmatter

1. Introduction

"Smart" hydrogels responding to external stimuli such as the temperature, pH, ionic strength, electric or magnetic fields have received great attention in recent years due to their potential applications in drug release, chemical separation, catalysis, surface modification, and other areas of actual interest.[1–3] Among thermosensitive hydrogels, poly (*N*-isopropylacrylamide) (PNIPAM) has been extensively investigated from both the aspects of basic characteristics[4,5] and applications[6,7] because of its unique structure characteristics, which makes the PNIPAM hydrogel exhibit a significant volume phase transition above the lower critical solution temperature (LCST), around 32 °C in aqueous media.[8,9] Therefore, the transition temperature is also called the volume phase transition temperature (VPTT). This transition phenomenon is related to the competition between two molecular effects: hydrogen bonding and hydrophobic interaction.[10] Below the VPTT, the PNIPAM gels are in a highly swollen state in water due to the hydrogen bonding between the amide groups and water molecules. However, when the temperature is raised above the VPTT, the polymer network collapses expelling most of its water due to the hydrophobic behaviour of the pendent isopropyl groups as well as that of the backbone. Tanaka *et al.*[11] demonstrated that the characteristic time for swelling and shrinking is proportional to the size of the gel. This means that the biggest disadvantage of macrogels (or bulk gels) is their slow response to the environment changes. However, this weakness can be overcome by preparing microgels that have the same structure as macrogels. This is because microgels with average diameters between 50 nm to several μm can respond to the environment considerably quickly. In addition, PNIPAM microgels can also be used as ideal model systems in soft condensed matter to investigate order–disorder,[12] glass

[a]*College of Chemistry, Beijing Normal University, Beijing 100875, China*
[b]*Department of Chemistry, The Chinese University of Hong Kong, Shatin, N. T. Hong Kong, China*

† Electronic supplementary information (ESI) available. See DOI: 10.1039/c4sm01516a

transitions[13] and polymer chain dynamics,[14] because they can be considered as deformable colloids.

It is well known that the volume phase transition is critically dependent on the gel composition; in particular, the internal structure, ionic concentration, pH, and solvent composition.[15] Therefore, it can be controlled by modifying the spatial distribution of cross-linking density, charge, and functional comonomer of the PNIPAM gel network. However, the general procedure of PNIPAM microgel synthesis leads to an inhomogeneous cross-linking density distribution, *i.e.*, microgels having a core–shell structure with a harder inner core and a softer shell. Although monodisperse PNIPAM microgel particles with a more homogenous cross-linking density distribution can be synthesised by a so-called "feeding method",[16] so far it is still unclear how the cross-linking density distribution affects the nature of the volume phase transition of PNIPAM microgels. Fernández-Barbero *et al.*[17] investigated the thermodynamics of swelling and the associated structure modifications of highly cross-linked PNIPAM microgels by small-angle neutron scattering (SANS) and dynamic light scattering (DLS), and found that the cross-linking density distribution has no effect on the volume phase transition of PNIPAM microgels. Their results were successfully described by the Flory–Rehner theory,[18] nonetheless, whether the inhomogeneity of the cross-linking density distribution will impact on the volume phase transition is still a puzzling issue because the theory deals with only homogeneous gel network.

A considerable effort has been made in the literature to gain insight into the relationship between the cross-linking density distribution and the volume phase transition of PNIPAM microgels.[16,19–21] Some reports suggest that the cross-linking density distribution plays an important role in the volume phase transition of microgels. For example; Wu *et al.*[9] compared the volume phase behavior of PNIPAM microgels to that of individual long linear PNIPAM chains and found that the crosslinked microgel particles have a higher transition temperature, but a less sharp phase transition than un-crosslinked polymer chains. This difference has been attributed to the polydispersity of the subchain length inside the microgels. Similarly, Tanaka and co-workers[15,22] suggested that the chains which are located in loosely crosslinked domains of the network considerably deform when the gel swells, whereas the chains in densely crosslinked domains almost have no contribution to swelling. On the other hand, Imre Varga *et al.*[16] have shown that the distribution of the cross-linking density within the particle does not affect the volume phase transition temperature of PNIPAM microgels, but markedly impacts on the swelling degree of the system. Furthermore, Sebastian Seiffert[19] compared the microgels that cross-linked uniformly on a nanometer scale to inhomogenous microgels and concluded that the inhomogeneity inside the polymer gel network hardly has an effect on the equilibrium swelling and shrinking, but it affects the deswelling kinetics dynamics of the volume phase transition. Recently, Wang *et al.*[4] studied the phase behavior and dynamics of PNIPAM microgel suspensions with different cross-linking densities by mechanical spectroscopy and found that the position of the VPTT is almost independent of the concentration and cross-linking density. Although these above studies more or less have provided the relationship between the structure and volume phase transition of gels, it is still hard to know the effect of the cross-linking density distribution on the volume phase transition, preventing rational optimization of these valuable functional microgels.

Technically, except for DLS, SANS and mechanical spectroscopy, as mentioned above, other methods are also used to study the volume phase transition of PNIPAM microgels. For example, Richtering *et al.*[23,24] studied the changes of viscosity and interfacial tension of PNIPAM microgels in the vicinity of the VPTT by means of rheology experiments. Sun *et al.*[25] proposed the chain collapse and revival thermodynamic mechanism of PNIPAM hydrogels by FT-IR. Martine Philipp *et al.*[26] used QENS to study the impact of the molecular dehydration process on the macroscopic changes in volume. Electrophoresis was carried out to identify the large morphology differences between PNIPAM microgels by Pelton and co-workers.[27] Dielectric relaxation spectroscopy, as a powerful tool to explore the polarization and dynamics inside materials, is increasingly used to study the dynamic and structural properties of both linear PNIPAM chains[28–31] and PNIPAM microgels.[32–34] Shikata *et al.*[28,29] investigated the temperature dependence of the hydration behavior of linear PNIPAM chains, and determined the number of hydrated water molecules per *N*-isopropylacrylamide and its change as the temperature. Marieke Füllbrandt *et al.*[30] monitored the "coil-to-globule" of linear PNIPAM by both the frequency and the temperature dependence of the conductivity spectra, and deduced the LCST and the critical overlap concentration as well as some other parameters from the dielectric spectra and the conformational changes of the PNIPAM chains. Nakano and co-workers[31] studied dielectric relaxation behavior of linear PNIPAM in protic and aprotic solvents as a function of polymer concentration, and pointed out that the molecular dynamics of PNIPAM chains is associated with the hydrogen bonding between PNIPAM chains and solvent molecules. Meanwhile, equipment to simultaneously measure of the optical and dielectric properties of linear PNIPAM and its hydrogels has been developed by Gómez-Galván,[32] from which the volume phase transition was monitored by measuring light transmittance, permittivity and the dielectric loss tangent as a function of temperature and the transition temperature is determined as 34.5 °C. Zhou *et al.*[33] have prepared three kinds of PNIPAM microgels with different charge and chain density distributions, and characterised the morphology and dielectric/electric properties of these microgels by DLS and dielectric spectroscopy. Further, in the recent study, Marieke Füllbrandt *et al.*[34] observed the collapse of PNIPAM microgels from the temperature dependence of conductivity spectra and attributed it to the interface polarization (MWS). They also discussed the relationship between the MWS effect and the crosslinking density, and established the correlation between the polarization effect and the swelling/deswelling ratio from DLS. The results of Zhou *et al.*[33] and Marieke Füllbrandt *et al.*[34] suggest that the volume phase transition temperature is irrelevant to the crosslinking density, but strongly depends on the spatial distribution of crosslinking

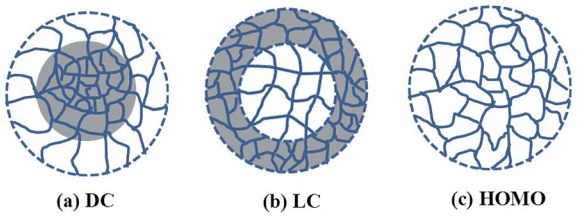

Fig. 1 Schematic of three types of PNIPAM microgels in a swollen state with different spatial cross-linking density distributions: (a) microgels with a dense core and a loose shell (DC), (b) microgels with a loose core and a dense shell (LC), and (c) microgels with homogenous cross-linking density distribution (HOMO). The darker the color, the higher the cross-linking density.

density; this is because that the dielectric behaviors in their studies present an bigger change around the VPTT for the microgels with a uniform chain density and charge distribution.

In the present work, we employed dielectric relaxation spectroscopy to study the volume phase transition behaviors of three types of PNIPAM microgels with different cross-linking density distributions. To this end, three kinds of microgels with a dense core and a loose shell (DC), with a loose core and a dense shell (LC), and with homogenous cross-linking density distribution (HOMO), as shown in Fig. 1, were used. Two well determined and temperature-dependence relaxations were observed by strict dielectric analysis. The relaxation mechanisms of the three types of microgel aqueous solution and the temperature dependency of the relaxation parameters were systematically analyzed. In particular, the modeling analysis for collapsing the microgel suspension was conducted, in order to deduce the effect of cross-linking density distribution on the volume phase transition of microgel particles. Moreover, we also expect to acquire some microscopic information on the volume phase transition of PNIPAM microgels.

2. Experimental section

2.1 Materials and preparation of the sample

2.2.1 Materials. *N*-isopropylacrylamide (NIPAM, Fluka) was recrystallized using a 1 : 1 toluene–*n*-hexane mixture twice. *N*,*N*-Methylene-bisacrylamide (MBA, Fluka) was recrystallized by using methanol, and potassium persulfate (KPS, Merck) was used as received. Deionized water was used in all the experiments.

2.2.2 Preparation of PNIPAM microgels. We have synthesized three types of nanometer-sized microgels with different spatial distributions of cross-linking density. By combining semibatch and temperature-programmed surfactant-free precipitation polymerization, the temperature-responsive PNIPAM microgels with a dense-core (DC), loose-core (LC), and homogeneous (HOMO) structure (see Fig. 1) were prepared. All the resultant microgels were centrifuged at a constant maximum centrifugal force of 6000*g* three times to remove the residual monomer and the un-cross-linked linear polymer fractions. The detailed preparation procedure can refer to the literature[35] and ESI.† Because the cross-linker content used to synthesize three types of microgels is the same, the only difference of these microgel particles is the spatial distributions of cross-linking density. In addition, no extra charge carriers have been added to the samples, only remaining charges coming from the polymerization process (*e.g.* from the initiator KPS). Even after extensive dialysis, a negative charge remains from the initiator. Therefore, the synthesized PNIPAM microgels possess a negatively charged surface, and potassium ions (K^+) are the main counterions in this system.

The three types of PNIPAM microgels mentioned above were dispersed into deionized water with the help of ultrasonication at room temperature (25 °C). The concentration of microgel aqueous solution used for dielectric measurement is 5 mg mL^{-1}.

2.2.3 Microgel characterization. The size of synthesized PNIPAM microgels was measured using dynamic light scattering (DLS). The apparatus used for DLS measurements was a modified commercial light-scattering spectrometer equipped with an ALV-5000 multi-τ digital time correlator and a He–Ne laser. Fig. 2 shows the temperature dependence of the mean hydrodynamic radius R_h for three PNIPAM microgels with different spatial cross-linking density distributions. As can be observed, R_h decreases gradually with temperature until a sharp but continuous volume transition from swollen to collapsed states takes place at the temperature of 32.5 °C, which is almost unaffected by the spatial distribution of cross-linking density.

2.2 Dielectric measurements

Dielectric measurements of PNIPAM microgels were carried out using a 4294A precision impedance analyzer (Agilent Technologies) over a frequency range from 40 Hz to 110 MHz and between 15 °C and 55 °C. A dielectric measuring cell with concentrically cylindrical platinum electrodes was employed to load the samples. The temperature of the samples is controlled by a circulating thermostatted water jacket. The applied alternating field was 500 mV. To eliminate the errors from the residual inductance (L_r) and stray capacitance (C_r) (the values of L_r, C_r and cell constant C_l have been determined by using three standard substances (air, ethanol and pure water) and KCl

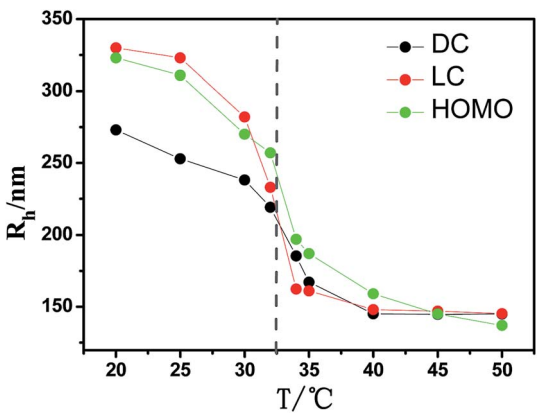

Fig. 2 Temperature dependence of the mean hydrodynamic radius for three types of PNIPAM microgels with different spatial cross-linking density distributions. The VPTT is indicated by a dashed vertical line.

solution of varying concentrations are 11.3 nH, 3.18 pF and 0.46 pF, respectively), the raw experimental data, capacitance C_x and conductance G_x were corrected according to Schwan's method from the following equations:[36]

$$C_s = \frac{C_x(1+\omega^2 L_r C_x) + L_r G_x^2}{(1+\omega^2 L_r C_x)^2 + (\omega L_r G_x)^2} - C_r \quad (1)$$

$$G_s = \frac{G_x}{(1+\omega^2 L_r C_x)^2 + (\omega L_r G_x)^2} \quad (2)$$

where C_s and G_s denote the modified capacitance and conductance, respectively. ω ($= 2\pi f$; f is the measurement frequency) is the angular frequency. Then the permittivity ε and conductivity κ were determined by equations $\varepsilon = C_s/C_l$ and $\kappa = G_s\varepsilon_0/C_l$ (ε_0 is the permittivity of vacuum), respectively.

2.3 Determination of relaxation parameters

The complex permittivity ε^* ($= \varepsilon - j\varepsilon''$, where ε and ε'' are permittivity and dielectric loss, respectively) of PNIPAM microgel aqueous solution under an applied electric field with angular frequency ω can be expressed as:

$$\varepsilon^*(\omega) = \varepsilon(\omega) - j\frac{\kappa(\omega)}{\omega\varepsilon_0} = \varepsilon(\omega) - j\left(\varepsilon''(\omega) + \frac{\kappa_l}{\omega\varepsilon_0}\right) \quad (3)$$

where κ_l is the low-frequency limit of conductivity (namely the low-frequency conductivity or dc conductivity) and $j = (-1)^{1/2}$. For aqueous solution systems with higher electrolyte contents like our samples, usually a considerable electrode polarization (EP) occurs in the lower frequency range. The conductivity of the whole system contains two contributions, one from the dc conductivity κ_l, and the other from the dielectric loss ε''. The dielectric loss was calculated from the conductivity spectra through the equation $\varepsilon''(\omega) = \frac{\kappa(\omega) - \kappa_l}{\omega\varepsilon_0}$, where κ_l was read out from the conductivity spectra at low frequency.

In our investigated frequency window, two remarkable relaxations were observed for each type of PNIPAM microgels. The following relaxation function including two Cole–Cole's terms and the electrode polarization term $A\omega^{-m}$ (A and m are adjustable parameters) was employed to analyze the experimental spectra:[37]

$$\varepsilon^* = \varepsilon_h + \sum_i \frac{\Delta\varepsilon_i}{1 + (j\omega\tau_i)^{\beta_i}} + A\omega^{-m} \quad (4)$$

where ε_h is the high frequency limit of permittivity; i is the number of dielectric relaxations ($i = 1, 2$ in this work); $\Delta\varepsilon_i$ and τ_i($= 1/(2\pi f_{0i})$, f_{0i} is the characteristic relaxation frequency) are the dielectric increment and relaxation time, respectively; β_i($0 < \beta_i \leq 1$) is the Cole–Cole parameter indicating the distribution of the relaxation time.

In order to determine the characteristic frequency clearly, the derivative dielectric loss ε''_{der} is presented on the basis of the logarithmic derivative of raw ε:[38,39]

$$\varepsilon''_{der}(\omega) = -\frac{\pi}{2}\frac{\partial\varepsilon(\omega)}{\partial \ln\omega} \quad (5)$$

This quantity displays a frequency dependence similar to that of the imaginary part of the complex permittivity ($\varepsilon''_{der}(\omega) \approx \varepsilon''(\omega)$), but, interestingly, the electrode contribution to ε''_{der} falls with frequency more rapidly than its contribution to ε''. Therefore, the logarithmic derivative method proves to be effective in separating relaxations from the EP effect and offers a good way to resolve overlapping relaxation peaks due to peak sharpening. Much work has been done in this respect, led by Delgado and co-workers.[38,40,41] By introducing the real part of eqn (4) into the derivative expression (eqn (5)), we get the following expression:

$$\varepsilon''_{der}(\omega) = \frac{\pi}{2}\left(\sum_i \frac{\beta_i(\Delta\varepsilon_i)(\omega\tau_1)^{\beta_i}\cos\left[\frac{\beta_i\pi}{2} - (1+\beta_i)\theta_i\right]}{1 + 2(\omega\tau_i)^{\beta_i}\cos\frac{\beta_i\pi}{2} + (\omega\tau_i)^{2\beta_i}}\right) + A\omega^{-m} \quad (6a)$$

$$\theta_i = \arctan\left[\frac{\sin\left(\frac{\beta_i\pi}{2}\right)}{(\omega\tau_i)^{-\beta_i} + \cos\left(\frac{\beta_i\pi}{2}\right)}\right] \quad (6b)$$

Eqn (6) has the same set of variables as that in eqn (4) and was used to fit the derivative dielectric loss curve in this work. First, we fitted the raw permittivity data using eqn (4) and determined the values of A and m. The EP effect was then subtracted from the raw permittivity data at each frequency by use of A and m. Then, the obtained new permittivity data $\varepsilon(\omega)$ were transferred into ε''_{der} using eqn (5) (solid circles in Fig. 3). Such relaxation parameters were determined by fitting the $\varepsilon''_{der} \sim f$ curve using eqn (6) without $A\omega^{-m}$. As a representative case, the frequency dependence of the derivative dielectric loss ε''_{der} for the HOMO microgel suspension at 30 °C was shown in Fig. 3. As can be clearly seen, two relaxations can be observed

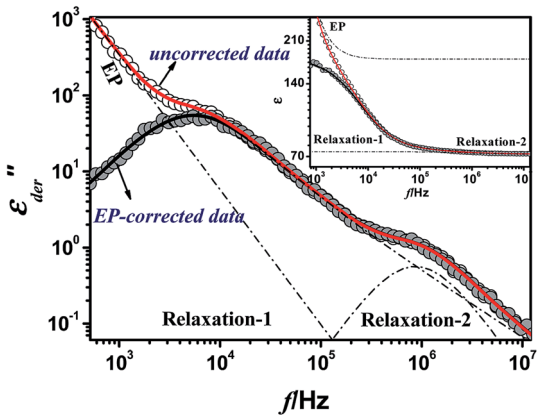

Fig. 3 Frequency dependence of the derivative dielectric loss of the HOMO PNIPAM microgel suspension at 30 °C. The inset shows the fitting result of the relative permittivity by using the same fitting parameters (except for the electrode polarization term) with eqn (4). The hollow circles are the uncorrected data and the solid circles are the corrected curves after subtraction of the EP effect. The solid lines represent the best fitting.

after subtracting EP (solid circles). The red solid line represents the best fitting curve with eqn (6), which is comprised of three parts: one is the EP effect which has been eliminated as shown by solid circles in Fig. 3, and two other parts are the contributions from the low- and high-frequency relaxation, respectively, *i.e.* relaxation-1 and relaxation-2 of Fig. 3. The inset of Fig. 3 shows the frequency dependency of raw permittivity (hollow circles) and that after eliminating the EP effect (solid circles).

3. Results and discussion

3.1 Dielectric behavior of PNIPAM microgels near the VPTT

Fig. 4 shows three-dimensional representations for the temperature dependence of the dielectric loss spectra for three types of PNIPAM microgels with different cross-linking density distributions in the temperature range of 15–55 °C. The data of these dielectric loss spectra are obtained according to the method described in Section 2.3, obviously the EP effect has been eliminated. The insets of Fig. 4 show the two-dimensional diagrams cut at the temperatures before (black curve) and after (red curve) the VPTT. It is clear from Fig. 4 that derivative dielectric loss spectra show two remarkable dielectric relaxation located at around 10^4 Hz and 10^6 Hz, called the low- and high-frequency relaxation, respectively. The relaxation strength (or dielectric increment) of low-frequency relaxation is much larger than that of high-frequency relaxation. Even more remarkable, the temperature dependence of $\varepsilon''_{der} - f$ of low-frequency relaxation changes markedly around 32 °C, and in other words, the dielectric increment of low-frequency relaxation declined sharply when the temperature rises to approach the VPTT of PNIPAM, but that of high-frequency relaxation change slightly, as shown in the inset of Fig. 4. This probably means that PNIPAM microgels have undergone a volume phase transition at this temperature.

3.2 Temperature dependence of permittivity in different frequency ranges

Moreover, the volume phase transition temperature is extremely well monitored by the temperature dependence of permittivity at the characteristic frequency, as seen in Fig. 5 which shows the permittivity ε of PNIPAM microgels, DC, LC, and HOMO as a function of temperature at the indicated frequencies of 338 Hz (low), 10.8 kHz (middle) and 1 MHz (high), respectively. It can be seen from Fig. 5(b) that no matter what kind of cross-linking density the microgel has, ε abruptly changes at ~32.5 °C (*i.e.* the VPTT) at a frequency of 10.8 kHz which is the characteristic frequency of low-frequency relaxation. At the frequencies below the characteristic frequency, the temperature dependence of permittivity ε shows no significant change near the VPTT, and ε increases monotonically with temperature rise, a case of 338 Hz is shown in Fig. 5(a). This is because the long-range migration motion of counterions coming from the polymerization process dominates the polarization occurring in the low frequency range. As the temperature increases, the increase of the ion mobility leads to ε due to this polarization increases, the increase of permittivity in the low frequency range as the temperature essentially belongs to electrode polarization and has nothing to do with bulk solution. In contrast, in the higher frequency range, ε decreases linearly as the temperature increases (see Fig. 5(c), a case of 1 MHz), this may be interpreted as: when temperatures rise, the random thermal motion of ions disturbed the bulk polarization which includes the micro-Brownian motions of PNIPAM chains and interfacial polarization. The orientation polarization of PNIPAM chains from micro-Brownian motions is restrained by random thermal motion of ions, meanwhile the ion distribution around microspheres is also disarranged, and as a result, the permittivity decided by above two factors decreases with temperatures rise. More importantly, for all three types of microgels, the temperature dependence of ε at middle frequency exhibits a sharp transition around the VPTT. This suggests that the structure of three samples has undergone great changes above and below the VPTT. Although the VPTT almost did not alter by the changes in the cross-linking density distribution, there are still some subtle differences in the temperature dependence behavior of permittivity for the three types of PNIPAM microgels. The relaxation processes in each frequency range will be further analyzed to obtain more information about the structure of the samples during the volume phase transition.

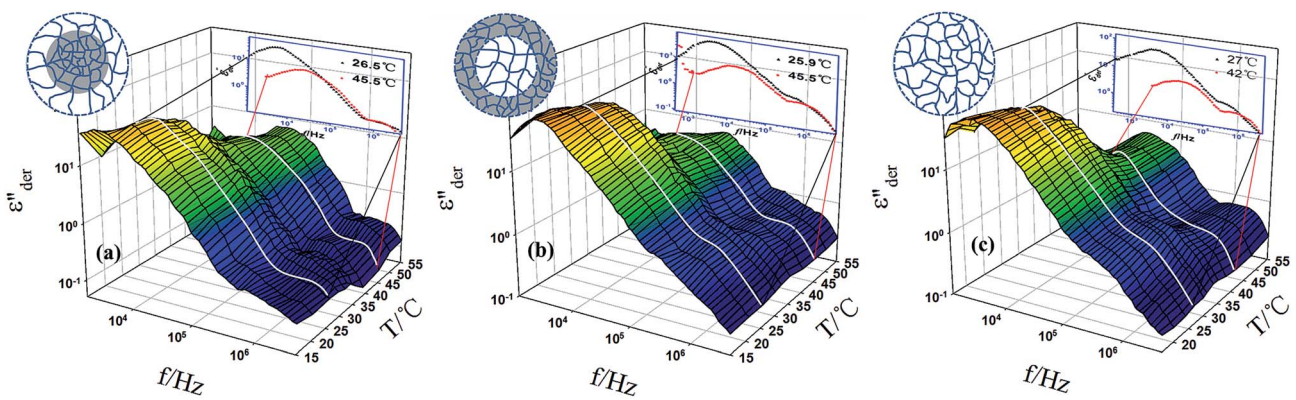

Fig. 4 Derivative dielectric loss ε''_{der} *versus* frequency and temperature in three-dimensional representations for three types of PNIPAM microgels with different cross-linking density distributions. The concentration of microgel suspension is 5 mg mL^{-1}. The inset shows the change of dielectric loss spectra above and below the VPTT.

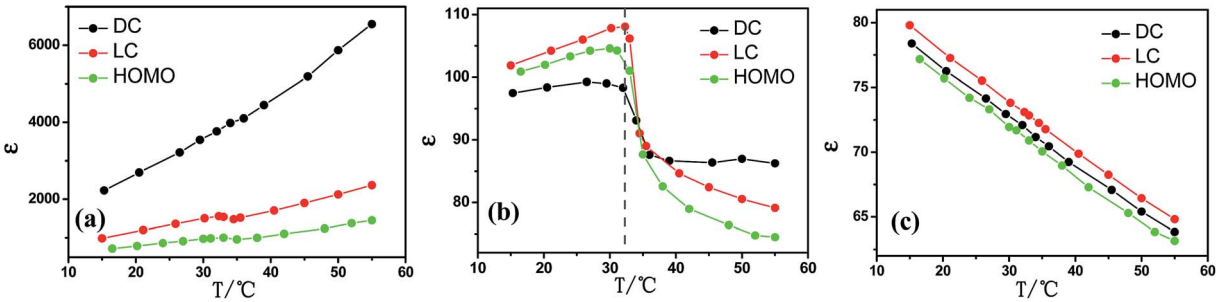

Fig. 5 Temperature dependence of permittivity for three types of PNIPAM microgels with different cross-linking density distributions at the indicated frequencies: (a) low frequency (338 Hz); (b) middle frequency (10.8 kHz); (c) high frequency (1 MHz). The concentration of the microgel suspension is 5 mg mL^{-1}. The VPTT is indicated by a dashed vertical line.

To accurately characterize the two relaxation processes and understand their causes, so that to examine the micro-mechanism of the volume phase transition in detail, it is necessary to determine the relaxation parameters, *i.e.* the dielectric increments, $\Delta\varepsilon_l$ $(= \varepsilon_l - \varepsilon_m)$ and $\Delta\varepsilon_h$ $(= \varepsilon_m - \varepsilon_h)$ and relaxation times, τ_l and τ_h of low- and high-frequency relaxations. The subscripts l, m, and h denote the low, medium and high frequency limit values, respectively. All these relaxation parameters were obtained by fitting the dielectric spectra in Fig. 4 applying eqn (6) including two Cole–Cole's terms (a typical example is shown in Fig. 3), which will be discussed in detail in the later sections.

3.3 Low-frequency relaxation: cross-linking density distribution and swelling capacity at low temperatures

3.3.1 Relaxation characteristics near the VPTT. A significant result is obtained by plotting the relaxation parameters of low-frequency relaxation *versus* temperature. Fig. 6(a) and (b) show the temperature dependence of dielectric increment $\Delta\varepsilon_l$ and relaxation time τ_l of low-frequency relaxation, respectively, for three types of PNIPAM microgels (DC, LC and HOMO). It is obvious from Fig. 6 that both $\Delta\varepsilon_l$ and τ_l for the three microgel solutions exhibit significant changes at the same temperature of 32.5 °C (*i.e.* VPTT), especially the value of $\Delta\varepsilon_l$ declined sharply at VPTT as well as τ_l. This is in good agreement with the results shown in Fig. 4 and 5(b). Another noteworthy feature is that the temperature dependence of $\Delta\varepsilon_l$ for microgels LC and HOMO was identical in the whole temperature range, but is very different from that of microgel DC when the temperature is below the VPTT, and the reasons will be discussed in detail in the following section.

It is remarkable that all these parameters show a sharp transition at ~32.5 °C for all three types of microgels, nearly independent of the cross-linking density distribution. However, previous studies indicate the cross-linking density distribution plays an important role in the volume phase transition of gels.[9,15,22] There exist two opposite opinions on this issue as mentioned in Introduction: Wu *et al.*[9] thought that the volume phase transition for inhomogeneous gel networks is less sharp than that of homogeneous networks, and only an average LCST (correspond to VPTT) can be given by the experiment. By contrast, Tanaka *et al.*,[15] thought that the gel swelling is essentially achieved by swelling of loosely crosslinked domains alone, therefore the volume phase transition should be more discontinuous (*i.e.* the volume phase transition becomes more obvious) if the gel network inhomogeneities are pronounced. Although neither opinions can be confirmed by the results in Fig. 6, it strongly suggests that the volume phase transition temperature, *i.e.* VPTT, is hardly influenced by the spatial distribution of cross-linking density, which is consistent with recent reports.[16,19] Furthermore, our results imply that three types of PNIPAM microgels with different cross-linking density distributions formed almost identical micro-architecture when the temperature is over the VPTT, which is not concerned with the temperature.

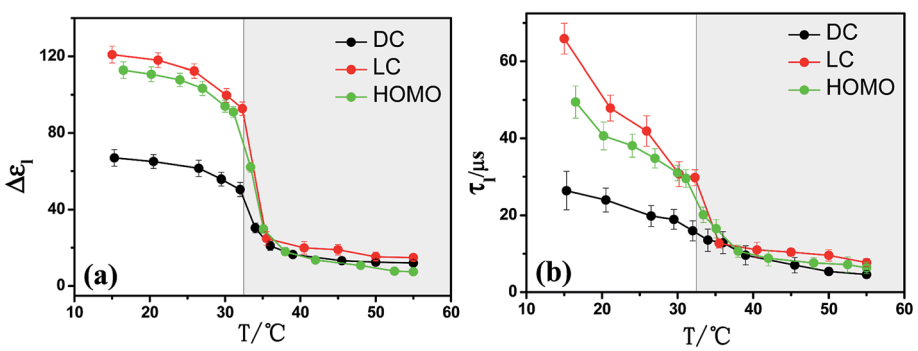

Fig. 6 Temperature dependence of the relaxation parameters of low-frequency relaxation: (a) dielectric increment and (b) relaxation time.

3.3.2 Relaxation mechanisms. Polyelectrolytes physics is always closely related to counterions. In the frequency range investigated, dielectric relaxation is expected to reveal the ion movements induced by the external electric field. Generally speaking, the dielectric relaxation spectroscopy of the linear macromolecular solution shows two relaxation processes: the high-frequency relaxation in the MHz frequency range and the low-frequency relaxation in the lower radio-wave range.[42] The former is due to the motion of free counterions which exist far from macroions, while the latter arises from the fluctuation of condensed counterions which exist in the vicinity of macroions. However, the dielectric behavior of microgels is usually much more complicated than that of linear macromolecular solution because of its network structure cross-linked by macromolecules. Osada *et al.*[43] investigated the dielectric relaxation of polyelectrolyte gels in a frequency range from 50 Hz to 110 kHz, and attributed the frequency around 10^3 to 10^4 Hz to the bound counterion fluctuation along the polymer network by crossing through the cross-linking points. By comparing with the linear polyelectrolyte solution, they pointed out that the motion of counterions in gel networks will be impeded by the cross-linking points, because of the energy barrier in cross-linking points. However, Cametti *et al.*[44] studied the dielectric properties of thermosensitive (dextran copolymer grafted with PNIPAM) hydrogels above and below the VPTT, and thought that the counterion fluctuation along the polymer chains by crossing through the insertion points of PNIPAM chains is a kind of movement in the short range, occurring at higher frequencies. But anyway, the characteristic length of this mechanism would not be comparable to the particle dimensions. We have tried to calculate the fluctuation length, based on the theory of counterion fluctuation,[43,44] but the calculation is similar to the hydrodynamic radius of microgel particles at each temperature. Therefore, we suggest that the low-frequency relaxation process in kHz to 10 kHz is caused by counterion polarization (*i.e.* counterions transport from one side of the spherical particle to the other side), which is the characteristic relaxation phenomenon at low frequency for aqueous colloidal systems. For counterion polarization, its relaxation time τ_l is controlled by the particle radius a, and the relationship between τ_l and a can be described as:[45]

$$\tau_l \approx \frac{a^2}{D} \tag{7}$$

where D $(= (RT/F^2)(\lambda/|z|)$, in which, R is the molar gas constant, T is the absolute temperature, F is the Faraday constant, λ is the molar conductivity, and z is the charge on the ion) is the diffusion coefficient and it increases by 2 to 3% per degree as the temperature increases from 25 °C.[46] n_B is the number concentration of condensed counterions, e is the elementary charge, and k_B is the Boltzmann constant. In our case of PNIPAM microgels, the counterions are mostly the potassium ions, introduced by the initiator of KPS in the polymerization.[35] Thus, the particle radius a of three types of microgels at different temperatures was estimated according to eqn (7) by using the relaxation time τ_l and diffusion coefficient D_K^+ $(= 1.957 \times 10^{-5}$ cm^2 s^{-1} at 25 °C),[46] as shown in Fig. 7. Interestingly, these estimates are remarkably in agreement with the measurement results by DLS (see Fig. 2). Because of this, the reduction of τ_l is related to the decrease of size upon shrinking.

We can now go back and think about the temperature dependence of the dielectric increment of low-frequency $\Delta\varepsilon_l$ as shown in Fig. 6(a). It is noted that the values of $\Delta\varepsilon_l$ at $T <$ VPTT are far larger than that at $T >$ VPTT, and $\Delta\varepsilon_l$ hardly changes with the temperature in the temperatures ranges of $T <$ VPTT, but it sharply drops when the temperature rises to the VPTT (32.5 °C). For counterion polarization, it is easy to understand that its dielectric increment also mainly depends on the particle size. Therefore, $\Delta\varepsilon_l$ at $T <$ VPTT is far larger than that at $T >$ VPTT due to the temperature dependence of the particle radius (refer to both Fig. 2 and 7). The significant decrease of $\Delta\varepsilon_l$ near the VPTT indicates a volume phase transition which has been confirmed by DLS and dielectric measurements.[9,28,29] The results above suggest that the volume phase transition of PNIPAM microgels is fairly quick and the transition temperature is located around 32.5 °C. A similar conclusion also can be obtained from the temperature dependence of the relaxation time in Fig. 6(b), although it is not as obvious as the dielectric increment.

In short, although the volume phase transition temperature was found to be almost independent of the spatial distribution of the cross-linking density and is located around 32.5 °C for all three types of microgels with different structures, the difference of cross-linking density distribution, *i.e.*, the structures between the three types of microgels discussed here were also reflected from both the low-frequency relaxation and DLS. We should note that all the analyzing results show that the particle sizes of both microgels HOMO and LC are larger than DC microgels in the temperature range of $T <$ VPTT. This means that the swelling capacity of microgels HOMO and LC are larger than microgel DC. The conclusion is supported by dynamic light scattering and light transmittance measurement,[16] on the other hand, it has been confirmed by small-angle neutron scattering that the swelling of the whole microgel particles is controlled by the shell evolution with temperature.[17] Therefore, we can conclude that the cross-linking density distribution has almost little

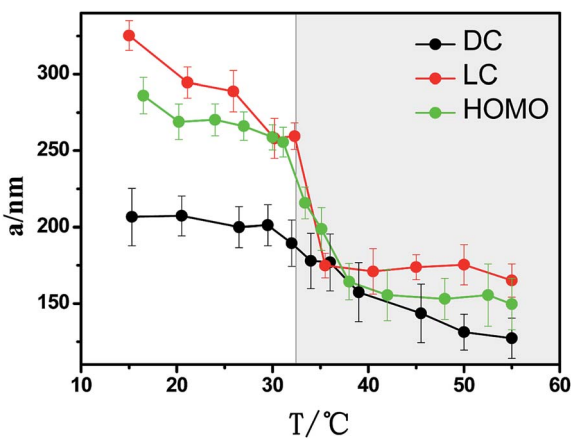

Fig. 7 Temperature dependence of the particle radius a of three types of microgels with different cross-linking density distributions.

effect on the volume phase transition temperature, but markedly impacts the swelling capacity of PNIPAM microgels in the lower temperature range.

3.4 High-frequency relaxation: hydration dynamic of microgels

Fig. 8 shows the temperature dependence of the dielectric relaxation parameters, dielectric increment $\Delta\varepsilon_h$ and relaxation time τ_h of high-frequency relaxation for three types of microgels with different cross-linking density distributions. Obviously, both $\Delta\varepsilon_h$ and τ_h show significant changes at the temperature of 32.5 °C (VPTT), which are very similar to those of low-frequency relaxation. Likewise, this is because PNIPAM microgels have undergone a volume phase transition near the VPTT, from a swollen coil conformation to a compact globular one along with the release of water molecules. Therefore, the change of microstructure for three types of microgels could also be reflected by high-frequency relaxation.

3.4.1 Relaxation mechanisms. We focus now on Fig. 6(a) and 8(a), it is obvious that the temperature dependence of $\Delta\varepsilon_h$ of high-frequency relaxation is completely different from that of low-frequency relaxation: as temperatures rise, $\Delta\varepsilon_h$ first increases and then decreases and shows a peak at around 32.5 °C (VPTT). This implies that the mechanism of high-frequency relaxation is different from that of low-frequency, and may be dominated by different polarization mechanisms above and below the VPTT, namely, there are at least two possible polarization modes which will contribute to the high-frequency relaxation. In the temperature region below the VPTT, microgels are in a highly swollen state in water and there is no clear interface between the microgel and water; as the temperature rises above the VPTT, the swollen microgel collapse into compact globules, expelling most of its water, correspondingly, the interface between the microgel globule and the continuous aqueous medium becomes much clear.

Based on the analysis above, the high-frequency relaxation can be considered to come from the contribution of two polarization modes: one is the local chain motion (also known as micro-Brownian motions) of PNIPAM chains, and the other originates from the interfacial polarization between microgel globules and medium water. At the temperatures below the VPTT, the former plays a dominant role, whereas when the temperature is above the VPTT, the interfacial polarization mainly contributes to the high-frequency relaxation process. The separate discussions about the two polarization modes are as follows:

(1) $T <$ VPTT

The dielectric increment $\Delta\varepsilon_h$ increases with temperature at $T <$ VPTT (see Fig. 8(a)); therefore the cause of the high frequency relaxation does not come from the contributions of the motion of free counterions and dipole orientation polarization because the dielectric increment decreases with the increase of temperature for these two kinds of polarization mechanisms. However, the polarization mode of the local chain motion of macromolecules can be detected in the MHz frequency range,[47–49] and its dielectric increment increases with temperatures.[50] Therefore, there is good reason to believe that the high-frequency relaxation around 10^6 MHz observed in the temperature range below the VPTT in this work is probably caused by the micro-Brownian motions of side groups of PNIPAM chains, or rather, is due to the random orientation of the *N*-isopropylamide groups (–ONHCH$(CH_3)_2$) of PNIPAM. The relaxation process therefore is closely associated with the hydrogen bonds between the amide groups and water molecules,[28,29,31] and the mechanism is shown in Fig. 9. At $T <$ VPTT, the microgels are in a highly swollen state and the PNIPAM chain exists in an expanded conformation due to intermolecular hydrogen bonding, which is not favorable for the random orientation of side groups (see Fig. 9(a)). However, as the temperature rises, parts of the hydrogen bonds fracture, this leads to the random orientation of side groups speed up, as a consequence, $\Delta\varepsilon_h$ increases with temperature and shows a maximal value when the temperature is near the VPTT. As the temperature is raised above the VPTT, hydrogen bonds fracture further and microgels collapse, and the random orientation of side groups becomes more difficult because of the intramolecular hydrogen bond of the polymer (see Fig. 9(b)), so $\Delta\varepsilon_h$ decreases with the increase of temperature.

According to the Debye–Stokes equation,[31,51] the relationship between the relaxation time τ_h and the solvent viscosity η_s for the micro-Brownian motions is given by:

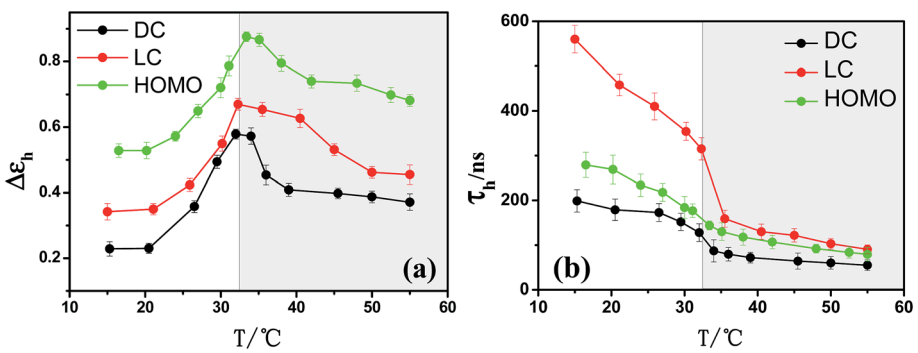

Fig. 8 Temperature dependence of the relaxation parameters of high-frequency relaxation: (a) dielectric increment and (b) relaxation time.

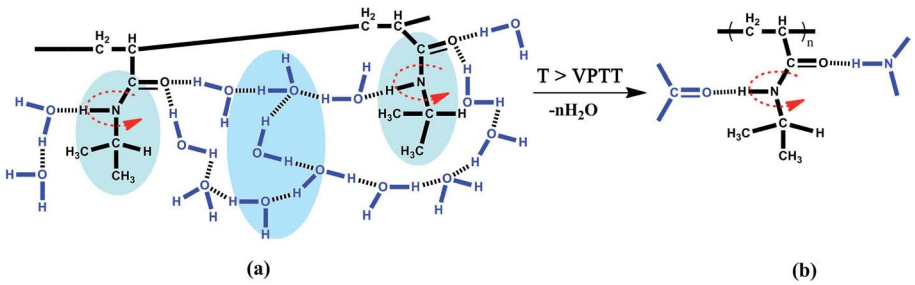

Fig. 9 Schematic illustration of the micro-Brownian motions of PNIPAM chains inside the microgels: (a) in the temperature range below the VPTT (*i.e.* microgels are in a highly swollen state), the PNIPAM chain stretches due to intermolecular hydrogen bonds between the amide groups and water molecules; (b) in the temperature range above the VPTT (*i.e.* microgels are in a collapsed state), the conformation of the PNIPAM chain becomes more compact due to the intramolecular hydrogen bond of the polymer. The red arrows represent the random orientation of side groups.

$$\tau_h = \frac{V}{k_B T}\eta_s \tag{8}$$

where V is the effective volume of a moving unit. Since the viscosity of solvent water η_s decreases with increasing temperature. According to eqn (8) the relaxation time τ_h for the random orientation of the side groups on PNIPAM chains decreases as the temperature increases, being consistent with the results shown in Fig. 8(b).

(2) $T >$ VPTT

In the temperature range above the VPTT, the PNIPAM microgels expel water and collapse, from a swollen coil conformation to a compact globular one, and the interface of microgel–water becomes clearer. This leads to a relative increase in the content of polymer molecules inside the gel microspheres. As a result, there is a significant difference of permittivity between microgel particles and water. Therefore, the high-frequency relaxation is importantly contributed by the interfacial polarization.

According to the Maxwell–Wagner interface polarization theory, the relaxation time τ_h (τ_{MW}) is given by:[52]

$$\tau_{MW} \propto \chi_D^2/D \tag{9}$$

where χ_D is the Debye length, equivalently the thickness of the electric double layer, and defined as:

$$\chi_D = \sqrt{\frac{\varepsilon_a \varepsilon_0 k_B T}{e^2 \sum_i C_i Z_i^2}} \tag{10}$$

where e, C and Z are the elementary charge, ion concentration, and the valence of ion, respectively. Since ε_a decreases slightly with increasing temperature, χ_D should also have a slight decrease as the temperature increases. χ_D was estimated using eqn (9) and τ_h was obtained experimentally and D_K^+ was obtained from the literature.[46] It is noteworthy that χ_D for the three types of microgels is only between ten and few tens of nanometres thickness, far less than the radius of microgels by DLS shown in Fig. 2. Besides, it decreases as the temperature increases, being consistent with the variation trend described by eqn (10). It is further demonstrated that the relaxation is caused by the interfacial polarization at temperature above the VPTT.

3.4.2 Modeling analysis for collapsing microgel particles. In the temperature range above the VPTT, PNIPAM microgels collapse, so, the collapsing microgel aqueous solution can be modeled as particle suspensions with complex permittivity ε^*, that is, the microgel particles with radius a and complex permittivity $\varepsilon_p^*(= \varepsilon_p - j\kappa_p/\omega\varepsilon_0)$ dispersed in a continuous aqueous medium with complex permittivity $\varepsilon_a^*(= \varepsilon_a - j\kappa_a/\omega\varepsilon_0)$ in a volume fraction ϕ, as shown in Fig. 10.

Based on the model above, the following Hanai's mixture equation,[53] which has been proved to give excellent simulations for various particle dispersions over a wide range of volume fraction up to 0.8, can appropriately describe the present collapsing microgel suspension:

$$\frac{\varepsilon^* - \varepsilon_p^*}{\varepsilon_a^* - \varepsilon_p^*}\left(\frac{\varepsilon_a^*}{\varepsilon^*}\right)^{1/3} = 1 - \phi \tag{11}$$

The phase parameters (ε_p, κ_p, ϕ and κ_a) described in the model are approximately related to the dielectric parameters (ε_m, κ_m, ε_h and κ_h) obtained experimentally which have been established by Hanai as follows:[53,54]

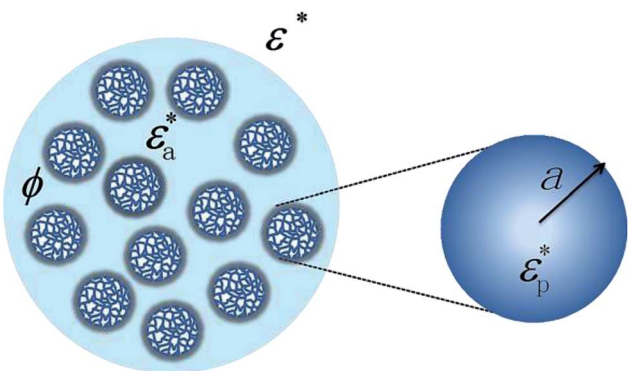

Fig. 10 Dielectric model of the PNIPAM microgel suspension at temperature of $T >$ VPTT.

$$\frac{\varepsilon_h - \varepsilon_p}{\varepsilon_a - \varepsilon_p}\left(\frac{\varepsilon_a}{\varepsilon_h}\right)^{1/3} = 1 - \phi \quad (12)$$

$$\kappa_h\left(\frac{3}{\varepsilon_h - \varepsilon_p} - \frac{1}{\varepsilon_h}\right) = 3\left(\frac{\kappa_a - \kappa_p}{\varepsilon_a - \varepsilon_p} + \frac{\kappa_p}{\varepsilon_h - \varepsilon_p}\right) - \frac{\kappa_a}{\varepsilon_a} \quad (13)$$

$$\varepsilon_m\left(\frac{3}{\kappa_m - \kappa_p} - \frac{1}{\kappa_m}\right) = 3\left(\frac{\varepsilon_a - \varepsilon_p}{\kappa_a - \kappa_p} + \frac{\varepsilon_p}{\kappa_m - \kappa_p}\right) - \frac{\varepsilon_a}{\kappa_a} \quad (14)$$

$$\frac{\kappa_m - \kappa_p}{\kappa_a - \kappa_p}\left(\frac{\kappa_a}{\kappa_m}\right)^{1/3} = 1 - \phi \quad (15)$$

Hence, we can determine the permittivities and conductivities of the collapsing microgel particles and solution as well as the volume fraction of the particles from the dielectric parameters using eqn (12)–(15) if the permittivity of the solution ε_a is given. The values of ε_a of varying temperatures can be calculated by the following equation:[46]

$$\varepsilon_a(T) = 78.3 \times [1 - 0.004579 \times (T - 25) + 0.0000119 \times (T - 25)^2 - 0.000000028 \times (T - 25)^2] \quad (16)$$

where the measured permittivity of doubly distilled water, at 25 °C, 78.3 was used. Thus, the phase parameters of three types of PNIPAM microgel particles of varying temperatures, ε_p, κ_p, ϕ, and κ_a were calculated from the high-frequency relaxation parameters, which will be discussed in detail below.

3.4.3 Temperature dependence of the phase parameters. Interestingly, all of the phase parameters exhibit an abrupt change around 32.5 °C, which reflects the basic characteristics of thermally sensitive PNIPAM microgels. For the sake of clarity, ϕ, κ_p, κ_a and ε_p are plotted against temperature in Fig. 11–13. Firstly, we focus on the temperature dependence of volume fraction ϕ of the microgel particles shown in Fig. 11. It is quite clear that ϕ presents an abrupt decrease at temperature of the VPTT, *i.e.* ϕ rapidly reduces from about 90% to 60%. Even with the doubtful accuracy of the values of ϕ at T < VPTT because the calculations of phase parameters below VPTT are only a rough approximation as mentioned above. Despite all this, the result ($\phi \approx 90\%$) still gives a defined and meaningful suggestion: most of the space of the microgel aqueous solution is occupied by the highly swollen gel balls in the temperature range below the VPTT. When the temperature rises above 32.5 °C, the result ($\phi \approx 60$–70% for the three microgels) is completely trusted because the model and calculations fit the collapsing microgel particle suspension. Therefore, the result of $\phi - T$ strongly supports the volume phase transition of the PNIPAM microgel: from a swollen coil conformation to a compact globular one, and proves the temperature of the phase transition to be almost independent of the cross-linking density distribution.

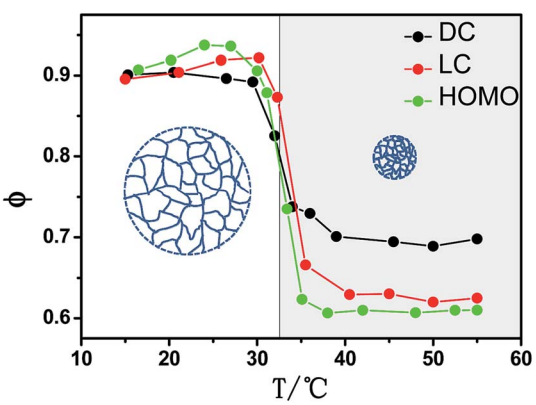

Fig. 11 Temperature dependence of the volume fraction of PNIPAM microgel particles.

Fig. 12 shows the plot of conductivities of continuous aqueous medium κ_a and microgel particles κ_p against the temperature for DC, LC and HOMO three types of microgels. Similarly, both κ_a and κ_p show a changeover point around the VPTT (see Fig. 12(b)), especially for κ_a. Moreover, the value of κ_p is much bigger than that of κ_a in the whole temperature range, this is because a small amount of charge is introduced into the PNIPAM microgels in the polymerization process. At T < VPTT, the microgels are in a highly swollen state in water, the κ_a almost remains a constant value with temperature rise and it increases linearly at higher temperature above the VPTT, suggesting that parts of the counterions are expelled from the microgels accompanied by the release of some associated water molecules from the isopropyl on PNIPAM. The monotonic increase in the conductivity of microgel particles κ_p over the whole temperature range suggests that the diffusion velocity of the counterions was accelerated as temperature rises.

Fig. 13 shows the temperature dependence of permittivity ε_p of PNIPAM microgel particles. It should be noted that the microgel particles still retain more than 80% of water even in a highly collapsed state, as has been confirmed by DLS,[9] and in the above dielectric model, ε_p represents the permittivity of the whole microgel particle which contains two contributions: one from the water inside and another from the PNIPAM polymer matrix with rather low permittivity. Therefore, it is easy to understand why the value of ε_p is always less than that of ε_a at each temperature. Moreover, the change of ε_p with the temperature has no significant difference from that of ε_a, especially at T < VPTT as shown in Fig. 13. Further, it is reasonable that both ε_a and ε_p decrease as the temperature increases from the view of dielectric physics.[55] Interestingly, an inflexion was found at the $\varepsilon_p - T$ curves for the three PNIPAM microgels when the temperature is close to 32.5 °C, *i.e.* VPTT, although not as dramatic. This shows that PNIPAM chains inside the microgels collapse and the water molecules bound to the hydrophobic isopropyl domains of PNIPAM are continually expelled from the microgels as temperature rises above the VPTT. As a result, the value of ε_p declined slightly compared to that at T < VPTT. It can also be noticed that the temperature dependence of ε_p for all microgels discussed here are not exactly the same. For the microgels with a loose core and a dense shell, *i.e.* LC, ε_p will not reduce anymore at T > VPTT. This may be expressed as: the collapsing microgel particles of LC may still keep the hollow structure and the water molecules trapped in the microgels form a relatively orderly structure, resulting in a larger dipole–dipole correlation,[56,57] so ε_p shows a value that is

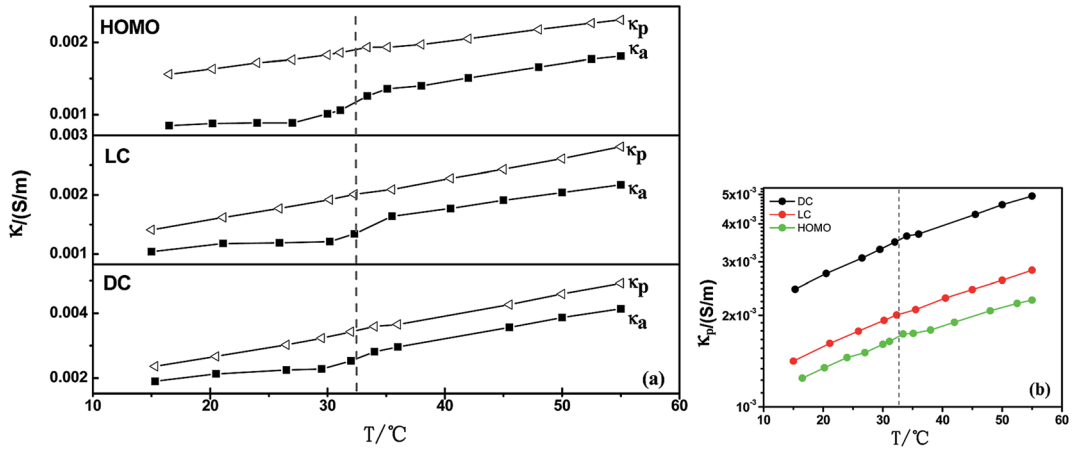

Fig. 12 (a) Temperature dependence of both the conductivity of PNIPAM microgel particles and continuous medium and (b) the temperature dependence of conductivity of PNIPAM microgel particles.

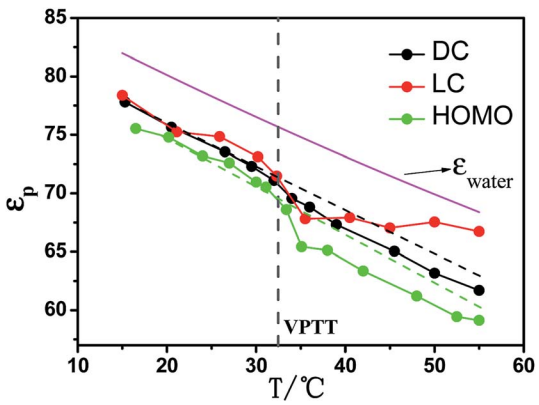

Fig. 13 Temperature dependence of permittivity of PNIPAM microgel particles. The dashed line is a guide to the eye only.

nearly free from the influence of the operation temperature at T > VPTT.

Apart from these above, we have also performed a thermodynamic analysis and estimated the activation enthalpy and activation entropy for the two relaxation processes observed in this work, according to the Eyring equation (see the ESI† in detail). This section will help us have a deeper insight into the dielectric relaxation behaviours and the changes in the microstructure inside the PNIPAM microgels during the volume phase transition. As was expected, the thermodynamic parameters and their temperature dependence strongly support the conclusions drawn from analyzing dielectric parameters and phase parameters.

4. Concluding remarks

Dielectric behaviors of three types of thermally sensitive PNIPAM microgels (*i.e.* DC, LC, and HOMO) with different cross-linking density distributions have been systematically studied in a frequency range from 40 Hz to 110 MHz at temperatures from 15 °C to 55 °C. By successfully removing the electrode polarization effect, two remarkable and unique relaxation processes were clearly observed. The temperature dependence of dielectric parameters for the low-frequency relaxation behaves differently from those of the high-frequency relaxation, but they all present an abrupt change around the VPTT for the all three types of microgels. Our results reveal that the spatial distribution of the cross-linking density has almost no effect on the volume phase transition temperature, but markedly affects the swelling capacity of PNIPAM microgels at low temperatures.

Relaxation mechanisms were proposed by detailed theoretical analysis, as summarized in the following diagram. The low-frequency relaxation is attributed to the counterion polarization in the whole measuring temperature range, whereas the high-frequency relaxation probably arises from the contributions of two parts: the local chain motions of PNIPAM (*i.e.* the micro-Brownian motions of the side group) at T < VPTT and the interfacial polarization at T > VPTT. The probable microstructures of PNIPAM microgels before and after phase transition were proposed.

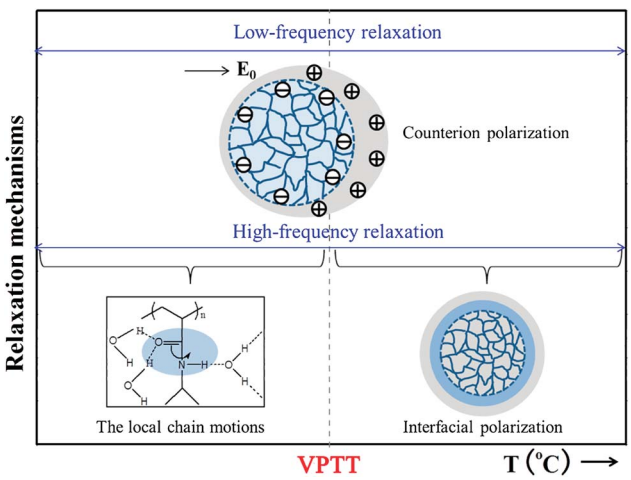

A model to describe the collapsing microgel suspension was proposed, based on which the phase parameters (ϕ, κ_p, κ_a and ε_p) were estimated by means of Hanai's equations. These parameters and their temperature dependence strongly support

the conclusions drawn from analyzing dielectric parameters. According to the Eyring equation, the activation enthalpy and activation entropy for the low- and high-frequency relaxation processes were estimated, which reconfirmed the changes in the microstructure inside the PNIPAM microgels during the volume phase transition.

This work helps to understand the relationship between the volume phase transition and the cross-linking density distribution near the VPTT, and will provide new insights into the micromechanism evolution inside the heterogeneous system. Particularly, the dielectric analysis based on the appropriate physical model is proven to be a promising tool to investigate the internal morphology and thermal behaviour in thermally sensitive microgel aqueous solution. In addition, the present study also can be taken as a starting point for further research on the polyelectrolyte networks.

Acknowledgements

This work was supported by the National Natural Scientific Foundation of China (Grant no. 21173025) and the Major Research Plan of NSFC (Grant no. 21233003).

References

1 R. Pelton, *Adv. Colloid Interface Sci.*, 2000, **85**, 1–33.
2 S. Nayak and L. A. Lyon, *Angew. Chem., Int. Ed.*, 2005, **44**, 7686–7708.
3 Z. Dai and T. Ngai, *J. Polym. Sci., Part A: Polym. Chem.*, 2013, **51**, 2995–3003.
4 H. Wang, X. Wu, Z. Zhu, C. Liu and Z. Zhang, *J. Chem. Phys.*, 2014, **140**, 024908.
5 S. Wongsuwarn, D. Vigolo, R. Cerbino, A. M. Howe, A. Vailati, R. Piazza and P. Cicuta, *Soft Matter*, 2012, **8**, 5857–5863.
6 Y. Hoshino, K. Imamura, M. Yue, G. Inoue and Y. Miura, *J. Am. Chem. Soc.*, 2012, **134**, 18177–18180.
7 F. d. r. Hapiot, S. p. Menuel and E. Monflier, *ACS Catal.*, 2013, **3**, 1006–1010.
8 M. Heskins and J. E. Guillet, *J. Macromol. Sci., Chem.*, 1968, **A2**, 1441–1455.
9 C. Wu, S. Zhou, S. C. Au-yeung and S. Jiang, *Angew. Makromol. Chem.*, 1996, **240**, 123–136.
10 F. Ilmain, T. Tanaka and E. Kokufuta, *Nature*, 1991, **349**, 400–401.
11 T. Tanaka and D. J. Fillmore, *J. Chem. Phys.*, 1979, **70**, 1214.
12 H. Senff and W. Richtering, *J. Chem. Phys.*, 1999, **111**, 1705.
13 E. Bartsch, M. Antonietti, W. Schupp and H. Sillescu, *J. Chem. Phys.*, 1992, **97**, 3950.
14 C. Wu and S. Zhou, *Macromolecules*, 1996, **29**, 1574–1578.
15 Y. Li and T. Tanaka, *Annu. Rev. Mater. Sci.*, 1992, **22**, 243–277.
16 R. Acciaro, T. Gilányi and I. Varga, *Langmuir*, 2011, **27**, 7917–7925.
17 A. Fernandez-Barbero, A. Fernandez-Nieves, I. Grillo and E. Lopez-Cabarcos, *Phys. Rev. E: Stat., Nonlinear, Soft Matter Phys.*, 2002, **66**, 051803.
18 P. J. Flory, *Principles of polymer chemistry*, Cornell University Press, New York, 1953.
19 S. Seiffert, *Macromol. Rapid Commun.*, 2012, **33**, 1135–1142.
20 H. Inomata, N. Wada, Y. Yagi, S. Goto and S. Saito, *Polymer*, 1995, **36**, 875–877.
21 K. Kratz, T. Hellweg and W. Eimer, *Polymer*, 2001, **42**, 6631–6639.
22 S. Hirotsu, Y. Hirokawa and T. Tanaka, *J. Chem. Phys.*, 1987, **87**, 1392.
23 Z. Li, W. Richtering and T. Ngai, *Soft Matter*, 2014, **10**, 6182–6191.
24 H. Senff and W. Richtering, *J. Chem. Phys.*, 1999, **111**, 1705–1711.
25 S. Sun, J. Hu, H. Tang and P. Wu, *J. Phys. Chem. B*, 2010, **114**, 9761–9770.
26 M. Philipp, K. Kyriakos, L. Silvi, W. Lohstroh, W. Petry, J. K. Krüger, C. M. Papadakis and P. Müller-Buschbaum, *J. Phys. Chem. B*, 2014, **118**, 4253–4260.
27 T. Hoare and R. Pelton, *Polymer*, 2005, **46**, 1139–1150.
28 Y. Ono and T. Shikata, *J. Am. Chem. Soc.*, 2006, **128**, 10030–10031.
29 Y. Ono and T. Shikata, *J. Phys. Chem. B*, 2007, **111**, 1511–1513.
30 M. Füllbrandt, R. von Klitzing and A. Schönhals, *Soft Matter*, 2012, **8**, 12116–12123.
31 S. Nakano, Y. Sato, R. Kita, N. Shinyashiki, S. Yagihara, S. Sudo and M. Yoneyama, *J. Phys. Chem. B*, 2012, **116**, 775–781.
32 F. Gómez-Galván, T. Lara-Ceniceros and H. Mercado-Uribe, *Meas. Sci. Technol.*, 2012, **23**, 025602.
33 J. Zhou, J. Wei, T. Ngai, L. Wang, D. Zhu and J. Shen, *Macromolecules*, 2012, **45**, 6158–6167.
34 M. Füllbrandt, R. von Klitzing and A. Schönhals, *Soft Matter*, 2013, **9**, 4464–4471.
35 M.-h. Kwok, Z. Li and T. Ngai, *Langmuir*, 2013, **29**, 9581–9591.
36 K. Asami, A. Irimajiri, T. Hanai and N. Koizumi, *Bull. Inst. Chem. Res., Kyoto Univ.*, 1973, **51**, 231–245.
37 S. Havriliak and S. Negami, *Polymer*, 1967, **8**, 161–210.
38 M. Jiménez, F. Arroyo, J. van Turnhout and A. V. Delgado, *J. Colloid Interface Sci.*, 2002, **249**, 327–335.
39 M. Wübbenhorst and J. van Turnhout, *J. Non-Cryst. Solids*, 2002, **305**, 40–49.
40 R. A. Rica, M. L. Jimenez and A. V. Delgado, *Soft Matter*, 2012, **8**, 3596–3607.
41 R. A. Rica, M. L. Jimenez and A. V. Delgado, *Soft Matter*, 2011, **7**, 3286–3289.
42 F. Bordi, C. Cametti and R. Colby, *J. Phys.: Condens. Matter*, 2004, **16**, R1423.
43 T. Mitsumata, J. P. Gong, K. Ikeda and Y. Osada, *J. Phys. Chem. B*, 1998, **102**, 5246–5251.
44 G. Masci and C. Cametti, *J. Phys. Chem. B*, 2009, **113**, 11421–11428.
45 C. Grosse and A. Delgado, *Curr. Opin. Colloid Interface Sci.*, 2010, **15**, 145–159.
46 D. R. Lide, *CRC Handbook of Chemistry and Physics*, CRC Press, Boca Raton, Florida, 2000.
47 S. Mashimo, P. Winsor IV, R. H. Cole, K. Matsuo and W. H. Stockmayer, *Macromolecules*, 1983, **16**, 965–967.

48 S. Mashimo, N. Miura, N. Shinyashiki and T. Ota, *Macromolecules*, 1993, **26**, 6859–6863.
49 R. Sengwa, S. Choudhary and S. Sankhla, *eXPRESS Polym. Lett.*, 2008, **2**, 800–809.
50 Y. Ishida, O. Amano and M. Takayanagi, *Kolloid-Z.*, 1960, **172**, 129–132.
51 P. Debye, *Polar Molecules*, Dover Publication, New York, 1929.
52 S. Dukhin, *Adv. Colloid Interface Sci.*, 1995, **61**, 17–49.
53 T. Hanai, *Kolloid-Z.*, 1960, **171**, 23–31.
54 T. Hanai and P. Sherman, *Emulsion Science*, Academic Press, New York, 1968.
55 J. Fang and Z. Yin, *Dielectric Physics*, Science Press, Beijing, 1989.
56 V. Ballenegger and J.-P. Hansen, *J. Chem. Phys.*, 2005, **122**, 114711.
57 J. Banys, M. Kinka, J. Macutkevic, G. Völkel, W. Böhlmann, V. Umamaheswari, M. Hartmann and A. Pöppl, *J. Phys.: Condens. Matter*, 2005, **17**, 2843.